

The rapid resetting of the Ca isotopic signatures of calcite at ambient temperature during its congruent dissolution, precipitation, and at equilibrium

Eric H. Oelkers^{1,2,*}, Philip A.E. Pogge von Strandmann^{2,3}, and Vasileios Mavromatis^{1,4}

¹Géosciences Environnement Toulouse (GET), CNRS, UMR5563, 14 Avenue Edouard Belin, 31400 Toulouse, France

²Earth Sciences, University College London, Gower Street, London WC1E 6BT, United Kingdom

³Department of Earth and Planetary Sciences Birkbeck, University of London, Gower Street, London WC1E 6DT, United Kingdom

⁴Institute of Applied Geosciences, Graz University of Technology, Rechbauerstrasse 12, 8010 Graz, Austria

Abstract- This study provides direct experimental evidence of the resetting of the calcium (Ca) isotope signatures of calcite in the presence of an aqueous fluid during its congruent dissolution, precipitation, and at equilibrium at ambient temperatures over week-long timescales. Batch reactor experiments were performed at 25 °C in aqueous NaCl solutions; air or CO₂-gas mixtures were bubbled through this fluid to fix pH. During congruent calcite dissolution, the fluid became enriched in isotopically heavy Ca, and the Ca isotope composition continued to become heavier after the fluid attained bulk chemical equilibrium with the mineral; the $\delta^{44/42}\text{Ca}$ composition of the fluid was up to 0.8 ‰ higher than the dissolving calcite at the end of the dissolution experiments. Calcite precipitation was provoked by increasing the reactor fluid pH after chemical equilibrium had been attained via dissolution. Rayleigh isotope fractionation effects were observed immediately after the pH was increased and rapid calcite precipitation occurred. However, isotopic exchange continued after the system chemically equilibrated, eradicating this Rayleigh signal. Taken together, these observations 1) confirm dynamic mineral-fluid equilibrium (i.e. dissolution and precipitation occur at equal, non-zero rates at equilibrium), and 2) indicate that isotopic compositions of calcite can readily equilibrate even when this mineral is in bulk chemical equilibrium with its coexisting fluid. This latter observation suggests the preservation of paleo-environmental isotopic signatures in calcite may require a combination of the isolation

* Corresponding Author: e-mail: e.oelkers@ucl.ac.uk; Telephone +44 (0)20 7673 5632

31 of fluid-mineral system from external chemical input and/or the existence of a yet to be
32 defined calcite dissolution/precipitation inhibition mechanism.

33

34

1. INTRODUCTION

35 The Ca isotope compositions of natural calcium carbonates are widely used to
36 illuminate a large number of natural processes including the global Ca cycle (Zhu and
37 Macdougall, 1998; Heuser *et al.*, 2005; Tipper *et al.*, 2006; Fantle and Tipper, 2014; Sawaki *et*
38 *al.*, 2014; Farkas *et al.*, 2016; Silva-Tamayo *et al.*, 2018), continental weathering rates (Tipper
39 *et al.*, 2008; Blattler *et al.*, 2011; Hindshaw *et al.*, 2011; 2013; Kasemann *et al.*, 2014), soil
40 formation (Page *et al.*, 2008; Cenki-Tok *et al.*, 2009; Holmden and Belanger, 2010), past and
41 present environmental conditions (Kasemann *et al.*, 2005; Owen *et al.*, 2016), and the
42 mechanism of biomineral formation (Pruss *et al.*, 2018). Moreover, the Ca isotope signatures
43 of natural waters are being used to trace their origin (Druhan *et al.*, 2013; Yan *et al.*, 2016;
44 Lyons *et al.*, 2017; Li *et al.*, 2018). These potential applications have motivated an increasing
45 number of studies focused on the measurement and behavior of calcium isotopic
46 compositions in low-temperature systems (e.g. DePaolo, 2004; Tang *et al.*, 2008, 2012;
47 Fantle and Tipper, 2014; Alkhatib and Eisenhauer, 2017; Wang *et al.*, 2017). A substantial
48 number of experimental studies have concluded that isotopically light Ca is preferentially
49 incorporated into calcium carbonate minerals (Lemarchand *et al.*, 2004; Marriott *et al.*,
50 2004; Gussone *et al.*, 2005, 2011; Reynard *et al.*, 2011; Tang *et al.*, 2008, 2012).

51 The interpretation of stable isotope compositions of natural minerals and waters
52 commonly relies on two assumptions. The first is that once a mineral is precipitated it retains
53 its original isotopic signal and thus preserves information about its formation conditions.
54 This assumption serves as the basis for paleo-environmental and paleo temperature

55 reconstructions (e.g. Marshall, 1992; Koch, 1998; Nagler *et al.*, 2000; Leng and Marshall,
56 2004; Fairchild *et al.*, 2006). The second assumption is that stable isotope signatures are
57 transferred conservatively to the fluid phase during congruent mineral dissolution¹ (e.g.
58 Jacobson and Holmden, 2008; Ryu *et al.*, 2011; Turchyn and DePaolo, 2011). This latter
59 assumption has been adopted to trace flow paths and the origin of fluids in natural systems
60 (e.g. Grazis and Feng, 2004; Wiederhold, 2015).

61 A number of studies, however, have presented evidence that the isotopic compositions
62 of carbonate minerals can be altered while dissolving stoichiometrically or when the mineral
63 is in bulk chemical equilibrium with the fluid phase over the course of hours to days. For
64 example, Pearce *et al.* (2012) observed that Mg isotopes fractionated substantially during
65 stoichiometric magnesite dissolution at 150 and 200 °C, and that the fluid Mg isotopic
66 composition continued to evolve after bulk equilibrium was attained between the mineral
67 and fluid. Mavromatis *et al.* (2016) reported that the Ba isotope signature of precipitated
68 witherite continued to evolve in closed system experiments after the attainment of bulk
69 mineral-aqueous fluid equilibrium. Mavromatis *et al.* (2017a) observed the continued Sr
70 isotope exchange in strontianite in closed system reactors after the attainment of bulk
71 mineral-aqueous fluid equilibrium in both dissolution and precipitation experiments. Similar
72 observations have been made for Mg isotope exchange in hydromagnesite (Oelkers *et al.*,
73 2018), Mg and Ca isotope exchange in dolomite (Perez-Fernandez *et al.*, 2017), Mg isotope
74 exchange in amorphous calcium carbonate (ACC) and Mg-rich calcite (Mavromatis *et al.*,
75 2017b), Ba isotope exchange in barite (Curti *et al.*, 2010), and Si isotope exchange in quartz
76 (Liu *et al.*, 2016). Mavromatis *et al.* (2012) and Shirokova *et al.* (2013) observed the

¹ The term congruent dissolution in this study refers to stoichiometric dissolution without the formation of secondary minerals nor evidence for re-crystallisation.

77 continuous re-equilibration of Mg isotopes between the hydrous Mg carbonate minerals
78 hydromagnesite/dypingite and its co-existing aqueous fluid at ambient temperatures during
79 experiments that lasted no more than 4 weeks. In a follow-up study, Mavromatis *et al.*
80 (2015) reported the continuous re-equilibration of C isotopes between the
81 hydromagnesite/dypingite and its co-existing aqueous fluid at the same conditions. The
82 resetting of mineral isotopic signatures in natural sedimentary rocks has been referred to as
83 'diagenetic effects'; a number of studies have concluded that these effects influence the
84 calcium isotopic signatures of natural calcium carbonate minerals (Fantle and DePaolo, 2007;
85 Teichert *et al.*, 2009; Fantle *et al.*, 2010; Druhan *et al.*, 2013; Fantle and Higgins, 2004;
86 Harouaka *et al.*, 2014; Jost *et al.*, 2014; Steefel *et al.*, 2014; Fantle, 2015; Chanda *et al.*,
87 2019).

88 Isotope exchange towards mineral-fluid *isotopic equilibrium* during congruent dissolution
89 and at *bulk chemical equilibrium* is consistent with the concept of dynamic equilibrium (van't
90 Hoff, 1884). This concept is often invoked for the interpretation of mineral dissolution and
91 precipitation rates (e.g. Aagaard and Helgeson, 1982; Oelkers *et al.*, 1994; Schott and
92 Oelkers, 1995; Oelkers, 2001; Schott *et al.*, 2009, 2012). Critical to the concept of dynamic
93 equilibrium as applied to mineral-fluid interaction is that chemical reactions proceed by two-
94 way mass transfer, the combination of forward dissolution and reverse precipitation. Note
95 that the reverse precipitation is of the identical material that is removed from the mineral
96 during forward dissolution. In undersaturated fluids, the rate of the forward dissolution is
97 faster than that of the reverse precipitation and the net overall process is mineral
98 dissolution, whereas in supersaturated solutions the rate of the reverse precipitation is
99 faster than that of forward dissolution and the overall net reaction is mineral precipitation.
100 At equilibrium, the rate of forward dissolution is equal to that of the reverse precipitation

101 such that there is no net bulk chemical transfer. As such, even if the original removal of an
102 element from a mineral via forward dissolution is isotopically conservative², isotopic
103 fractionation can occur as a consequence of the coupled reverse precipitation, both during
104 bulk dissolution and at equilibrium (see Steefel et al., 2014). To assess the degree to which
105 such processes can effect the isotopic compositions of calcite, this study followed the
106 temporal evolution of calcium isotope compositions of the fluid phase during the congruent
107 dissolution, precipitation, and at chemical equilibrium during ambient temperature closed-
108 system calcite-water experiments. Results of shorter than month-long experiments
109 demonstrate that 1) calcium isotopes are not conservatively transferred the fluid during
110 congruent calcite dissolution, 2) the calcium isotopic composition of calcite and its co-
111 existing fluid phase continue to evolve after the fluid has attained bulk chemical equilibrium,
112 and 3) kinetically mediated isotopic signatures obtained during rapid calcite precipitation
113 can be subsequently re-equilibrated by further fluid-calcite interaction. These observations
114 require that a substantial portion of the calcium within the calcite is transferred in and out of
115 the fluid phase in experiments performed at conditions at or near to calcite/aqueous fluid
116 bulk chemical equilibrium over the course of only a few weeks. The purpose of this article is
117 to report the results of this experimental study and use these to assess the potential for the
118 preservation of the original calcium isotope compositions of calcite in natural systems.

119

120 **2. COMPUTATIONAL, EXPERIMENTAL, AND ANALYTICAL METHODS**

121 The standard state adopted in this study for thermodynamic calculations is that of
122 unit activity for pure minerals and H₂O at any temperature and pressure. For aqueous

² The term isotopically conservative in this manuscript refers to the transfer of a metal to an aqueous solution without zero isotopic fractionation.

123 species other than H₂O, the standard state is unit activity of the species in a hypothetical 1
124 molal solution referenced to infinite dilution at any temperature and pressure. Calcite
125 dissolution can be described using:



127 Taking account of the standard state, the law of mass action for this reaction is given by:

$$128 K_{\text{calcite}} = a_{\text{Ca}^{2+}} a_{\text{CO}_3^{2-}} \quad (2)$$

129 where K_{calcite} stands for the equilibrium constant of reaction (1), and a_i represents the
130 activity of the subscripted aqueous species. The saturation state of an aqueous fluid with
131 respect to calcite can be quantified using the saturation index (SI) defined by

$$132 SI = \log\left(\frac{IAP}{K_{\text{calcite}}}\right)$$

133 where IAP signifies for the aqueous ion activity product for reaction (1). Note that SI is
134 negative when the fluid is undersaturated with respect to calcite, positive when
135 supersaturated, and zero at fluid-calcite equilibrium. All thermodynamic calculations in this
136 study were performed using the PHREEQC computer code, together with its minteq.v4
137 database (Parkhurst and Appelo, 1999). Note that consideration of the analytical
138 uncertainties described below and those associated with the equilibrium constants present
139 in the minteq.v4 database, uncertainties associated with the calcite SI values calculated in
140 this study are on the order of ± 0.1 (c.f. Voigt et al., 2018).

141 Two calcite-aqueous fluid batch reactor experiments were performed in 1000 ml
142 polypropylene reactors that were placed in a thermostated bath operating at 25 °C. Batch
143 reactor systems were chosen for this study to allow the fluid-water system to attain close to
144 bulk chemical equilibrium conditions, such that the isotopic evolution of the calcite and its

145 coexisting fluid phase could be observed in the absence of net chemical transfer between
146 the mineral and the fluid. Each batch reactor was equipped with a floating stirring bar that
147 rotated at ~250rpm. Experiment A was initiated by placing 2.35 g of calcite seed crystals
148 together with 965.4 g of an aqueous 0.01 mol/kg NaCl solution into the reactor. Air was
149 bubbled continuously through the reactor to fix pH. After 25 hours, the air was replaced by
150 pure CO₂ gas, lowering the fluid pH to 6.2 and provoking calcite dissolution; this part of
151 experiment A is referred to as the 'dissolution leg'. After an additional 193 hours, the pure
152 CO₂ gas was replaced with a 1% CO₂/N₂ gas mixture, raising the pH to 7.5 and provoking
153 calcite precipitation; this part of experiment A will be referred to as the 'precipitation leg'.
154 Experiment B was initiated by placing 2.03 g of calcite crystals, together with 1001.1 g of a
155 0.008 mol/kg NaCl solution into a reactor. Pure CO₂ gas was bubbled in the reactor fluid,
156 leading to a fluid pH of 6.3 and provoking calcite dissolution. Fluid samples were collected
157 regularly from each reactor using a 0.45 µm cellulose nitrate syringe filter. Prior to sampling,
158 the stirring bar was stopped to allow the suspended calcite to settle, minimizing changes in
159 the mass of solid present in the reactor due to sampling; no evidence of calcite passing
160 through the filter syringes during the sampling was observed. Note also that prior to their
161 introduction in the reactors, all gasses were saturated with a 0.01 mol/kg NaCl solution in a
162 separate fluid cell to avoid fluid evaporation in the reactors.

163 The solids used in these experiments were pure synthetic Merck reagent grade
164 calcite. The calcite used in the two experiments was taken from different containers of
165 Merck calcite, so differed slightly in their initial Ca isotope compositions (see below). Pure
166 synthetic calcite was chosen for these experiments to avoid any potential artifacts (such as
167 non-congruent dissolution) arising from the presence of impurities in the solids. Note that,
168 for example, the presence of Mg in biogenic calcite can provoke the dissolution of the

169 original solid and the precipitation of a more stable Mg-free calcite during isotope exchange
170 experiments (Chanda et al., 2019). The solids in our study were not cleaned prior to use to
171 avoid altering the surfaces prior to the experiments. The synthetic calcite consisted of 4 to
172 15 μm rhombohedral shaped crystals as shown in Fig. 1. X-ray Diffraction (XRD) and Energy
173 Dispersive X-ray Spectroscopic (EDS) analyses confirmed that these crystals were pure
174 calcite. Potential isotopic heterogeneities in these solids were not investigated. The specific
175 surface area of the original calcite, as determined by multi-point krypton adsorption
176 according to the BET method (Brunauer *et al.*, 1938) using a Quantachrome Instruments
177 Autosorb 1, was $0.25 \pm 10\% \text{ m}^2/\text{g}$.

178 Aqueous fluids were regularly sampled from the reactor and analyzed for total
179 alkalinity, pH, and calcium concentration. The alkalinity of each fluid sample was obtained by
180 HCl titration using an automatic Schott TitroLine alpha TA10^{plus} titrator with an uncertainty
181 of $\pm 2\%$ and a detection limit of $5 \times 10^{-5} \text{ eq kg}^{-1}$. Fluid phase pH measurements were
182 performed at $25 \text{ }^\circ\text{C}$ immediately after sampling using a standard glass electrode, previously
183 calibrated with 4.01, 6.86, and 9.18 NIST pH buffers; the precision of these measurements is
184 $\pm 0.02 \text{ pH}$ units. The Ca concentration of each sample was measured by flame Atomic
185 Absorption Spectroscopy (AAS) with an analytical uncertainty of $\sim 3\%$ and a detection limit of
186 $6 \times 10^{-7} \text{ M}$. The estimated uncertainties in these analyses are based on repeat analyses of
187 selected samples performed regularly during the analyses.

188 The calcium isotope compositions of the fluid samples, as well as the bulk solids
189 before and after the experiments were determined. Calcium isotope compositions are
190 reported as $\delta^{44/42}\text{Ca}$ normalized to the NIST Ca standard SRM915a (Schmidt *et al.*, 2001)
191 consistent with

192
$$\delta^{44/42}\text{Ca} = \{[(^{44}\text{Ca}/^{42}\text{Ca})_{\text{sample}} - (^{44}\text{Ca}/^{42}\text{Ca})_{\text{standard}}]/(^{44}\text{Ca}/^{42}\text{Ca})_{\text{standard}}\} \times 1000 ,$$

193 where $(^{44}\text{Ca}/^{42}\text{Ca})_{\text{sample}}$ refers to the indicated isotopic molar ratio of the subscripted phase.
194 Calcium was purified for isotopic analysis by ion exchange chromatography. Prior to
195 separation, fluid samples were evaporated to dryness in a Savillex beaker, redissolved in
196 concentrated aqueous HNO_3 , evaporated to dryness again and dissolved in aqueous 2M HCl
197 ready for loading on columns. For the solid calcite samples, ~ 10 mg of the solid was
198 dissolved in concentrated aqueous HCl before being evaporated to dryness, then dissolved
199 in concentrated aqueous HNO_3 , evaporated to dryness again then dissolved in aqueous 2M
200 HCl. An aliquot of this fluid was subsequently loaded onto the ion exchange resin, with 20–
201 30 μg of Ca processed for each sample. Purification chemistry was performed in the isotope
202 laboratories in the Earth Science Department at Oxford University. The method was
203 previously described (Chu *et al.*, 2006; Reynard *et al.*, 2010; Blattler *et al.*, 2011), but, briefly,
204 samples were purified through a 2-step ion-exchange method to isolate Ca^{2+} , where the first
205 column used AG50W X12 (200-400 mesh) cation exchange resin, and the second column a Sr
206 spec resin, to separate the isobaric interferences from strontium. Total Ca yields were
207 greater than 99%, as determined by Ca content analysis of splits collected before and after
208 the main collection bracket. The total procedural blank for Ca isotope analysis is ~ 0.5 – 0.7 ng,
209 which is insignificant compared to the mass of sample used. Purified fluids were diluted to a
210 concentration of 10 $\mu\text{g}/\text{ml}$, and measured on a Nu Instruments multi-collector inductively
211 coupled plasma mass spectrometer (MC-ICP-MS), using a sample-standard bracketing
212 system relative to SRM-915a. With an uptake rate of 100 $\mu\text{l}/\text{min}$, and using a Nu Instruments
213 DSN desolvating nebulizer, a sensitivity of ~ 40 pA on ^{44}Ca was achieved. Mass 43.5 was
214 continuously monitored to assess potential doubly charged Sr; the contribution of Sr to the
215 Ca isotope ratio was consistently less than 0.01%. Instrument precision was assessed by

216 running in-house Ca standards, and accuracy and external precision was assessed by
217 repeated analyses of seawater ($\delta^{44/42}\text{Ca} = 0.96 \pm 0.11\text{‰}$ ($n=8$, chemistry=7), in keeping with
218 previously cited long-term reproducibility (Reynard *et al.*, 2011). The uncertainties in
219 measured isotopic analyses are given as two standard deviations of repeated analyses.

220

221

3. Results

222 The temporal evolution of the chemical and isotopic composition of the fluid, as well
223 as the mass of fluid remaining in the reactor after each sample in experiments A and B are
224 listed in Tables 1 and 2; the temporal evolution of Ca concentration and isotopic composition
225 during these experiments are shown in Figs. 2 and 3. The $\delta^{44/42}\text{Ca}$ of the original calcite
226 grains in experiment A was $-0.25 \pm 0.08\text{‰}$. The dissolution of calcite during the first 25 hours
227 of the experiment performed in an aqueous 0.01 mol/kg NaCl solution leads to a fluid phase
228 Ca concentration of 0.22×10^{-3} mol/kg and a $\delta^{44/42}\text{Ca}$ of $0.01 \pm 0.03\text{‰}$; this latter value is
229 0.26‰ greater than that of the dissolving calcite. The fluid phase is calculated to be slightly
230 supersaturated with respect to calcite at this time, which may be the result of either
231 analytical uncertainty on the pH, alkalinity, and aqueous Ca measurements, and/or due to
232 the presence of minor high-energy surfaces or ultra fine particles, unobserved by SEM, in the
233 original calcite powder. The reactor fluid was then bubbled with pure CO_2 , which decreased
234 its pH to 6.2 and provoked further calcite dissolution. The fluid phase Ca concentration
235 increased to $\sim 4.5 \times 10^{-3}$ mol/kg after ~ 96 hours of elapsed time then remained close to
236 constant. The saturation state of the reactive fluid was no greater than 0.09 from this time
237 until the end of this experiment, consistent within uncertainty of calcite equilibrium. The
238 isotopic composition of the fluid phase, however, evolved continuously during this

239 dissolution leg of the experiment. The $\delta^{44/42}\text{Ca}$ of the fluid phase was $0.34\pm 0.06\text{‰}$ 23 hours
240 after the pH change; this increased to $0.57\pm 0.01\text{‰}$ before the fluid pH was increased after
241 218 hours of elapsed time. These values are 0.45‰ and 0.72‰ greater than the initial
242 dissolving calcite. Changing the bubbling gas in the reactor to a CO_2/N_2 mixture after 218
243 hours increased the fluid pH to 7.5 leading to calcite precipitation. Calcite precipitation
244 lowered the fluid phase Ca concentration to 1.8×10^{-3} mol/kg; this concentration was
245 constant and within analytical uncertainty of calcite-fluid equilibrium for the final 140 hours
246 of the experiment. Despite the fact that the fluid phase was in chemical equilibrium with
247 calcite over this period, the fluid-phase Ca isotopic composition evolved substantially. The
248 fluid phase $\delta^{44/42}\text{Ca}$ first increased from 0.57 ± 0.01 to $1.15\pm 0.04\text{‰}$ after the onset of
249 precipitation, then decreased to $\sim 0.8\text{‰}$ at the end of the experiment. Mass balance
250 calculations indicate that after calcite dissolution during the dissolution leg, 18% of the Ca in
251 the system was in the fluid phase. This was lowered to 9% during the precipitation leg.

252 The evolution of the fluid phase composition of experiment B is shown in Fig. 3. The
253 $\delta^{44/42}\text{Ca}$ of the original calcite grains in experiment B, which were obtained from a distinct
254 container of Merck reagent grade calcite as that of experiment A, was $0.12\pm 0.07\text{‰}$. The
255 fluid in this experiment was constantly bubbled with pure CO_2 such that the fluid pH
256 remained at a near constant 6.3. Calcite dissolved rapidly, the fluid phase attained a Ca
257 concentration of 9.5×10^{-3} mol/kg, consistent, within uncertainty, with calcite equilibrium,
258 after less than 28 hours and remained near this concentration through the end of the
259 experiment. The isotopic composition of the fluid, however, increased with time throughout
260 the experiment, increasing from $0.22\pm 0.06\text{‰}$ to $\sim 0.6\text{‰}$ after the aqueous Ca concentration
261 attained a close to constant value at near to calcite-fluid chemical equilibrium conditions.
262 These fluid Ca isotopic compositions are substantially heavier than that measured in the

263 solid calcite before and after the experiment. After calcite-fluid equilibrium was attained,
264 roughly 45% of the Ca in the system was present in the fluid phase.

265 Photomicrographs of the calcite following experiments A and B are shown in Fig 1. In
266 both cases only calcite is present in the post-experiment solids. Similarly post-experiment
267 analysis of the solids recovered from these experiments by XRD revealed the presence of
268 only calcite. The calcite recovered from experiment B shows the effect of dissolution;
269 dissolution appears to be driven by the removal of material from the corners of calcite
270 crystals rather than due to the formation of etch pits. This behavior is consistent with
271 dissolution occurring at near to equilibrium conditions where there is insufficient driving
272 force to create etch pits. Note also that as 45% of the calcite dissolved during experiment B
273 is it possible some of the smaller grains dissolved completely. The calcite recovered from
274 experiment A has far fewer steps than that recovered from experiment B, likely due to the
275 precipitation of calcite onto pre-dissolved grains.

276

277

4. Discussion

278 ***4.1 Isotope release during congruent calcite dissolution and at bulk equilibrium***

279 Results indicate that Ca isotopes fractionated during congruent calcite dissolution.
280 Evidence that calcite dissolved congruently during the dissolution experiments include 1) the
281 results of thermodynamic calculations demonstrating that the fluid phase was either
282 undersaturated or in equilibrium within uncertainty with respect to calcite, and
283 undersaturated with respect to other potentially precipitating phases during the dissolution
284 leg of experiment A, and throughout experiment B, and 2) the SEM images after the
285 experiments indicate the presence of only calcite in the solid phase. Moreover, the temporal

286 evolution of reactive fluid Ca concentrations calculated using calcite dissolution and
 287 precipitation rates reported by Chou *et al.* (1989) together with calcite solubility constants
 288 generated using PHREEQC match closely those measured in the reactors (See Figs 2a and
 289 3a). As a result of calcite dissolution in experiment A, the measured $\delta^{44/42}\text{Ca}$ of the fluid
 290 phase evolved to $0.57\pm 0.01\text{‰}$ compared to the $\delta^{44}\text{Ca}$ of $-0.25\pm 0.08\text{‰}$ of the original calcite.
 291 The change in the Ca isotopic composition of the calcite due to dissolution in experiment A
 292 was not determined directly; although the Ca isotopic composition of the final solids
 293 recovered from this experiment was measured, these solids experienced both dissolution
 294 and subsequent precipitation. Nevertheless, because the experiment initially consisted of
 295 calcite and a Ca-free fluid phase, the change in the calcite bulk Ca isotope composition
 296 during this experiment can be computed from the measured isotopic composition of the
 297 fluid phase via mass conservation taking account of

$$298 \quad \delta^{44/42}\text{Ca}_{\text{initial solid}}m_{\text{Ca,initial solid}} = \delta^{44/42}\text{Ca}_{\text{solid}}m_{\text{Ca,solid}} + \delta^{44/42}\text{Ca}_{\text{fluid}}m_{\text{Ca,fluid}} \quad (3)$$

299 where $m_{\text{Ca},i}$ refers to the mass of calcium in the *i*th phase, and the subscripts *initial solid*,
 300 *solid*, and *fluid* designate the original solid, and the solid and fluid phase present in the
 301 reactor at the time of interest. This calculation was performed iteratively using an excel
 302 spreadsheet using the data summarized in Table 1. At each time interval, delineated by the
 303 sampling times, the Ca isotope composition of calcite was determined taking account of the
 304 mass and composition of the fluid remaining in the reactor and that removed by sampling
 305 over time. This calculation indicates that following just the ‘dissolution leg’ of experiment A,
 306 the bulk calcite obtains a $\delta^{44/42}\text{Ca}$ of -0.42‰ , a decrease of 0.17‰ during 9 days of calcite-
 307 fluid interaction at ambient temperature. The decrease between the bulk $\delta^{44/42}\text{Ca}$ of the
 308 calcite before and after the 8 days of dissolution during experiment B was measured directly

309 and determined to be 0.19‰. The degree to which the calcite was isotopically homogeneous
310 was not determined either before or after the experiments. It is also possible that Ca
311 isotopes are heterogeneously distributed in the solids at the end of the experiments due to
312 sluggish solid-state transport rates. Note that although isotopic heterogeneities in the solid
313 phase could have accounted for the difference in isotopic compositions between the bulk
314 original calcite and the reactive fluid during the first ~24 hours of the dissolution leg of
315 experiment A and experiment B, the calcium isotope compositions of the reactive fluids
316 continued to increase after this fluid attained chemical equilibrium with respect to calcite.

317 The exact mechanism by which isotopes fractionate during congruent calcite
318 dissolution and at equilibrium is somewhat uncertain. Either some mechanism must allow
319 isotopically heavy Ca to be preferentially released from the calcite structure during forward
320 dissolution or lighter calcium needs to be returned from the fluid to the calcite during
321 reverse precipitation. The first mechanism seems rather unlikely, as earlier work on mineral
322 dissolution suggest that in both carbonates and silicate minerals, lighter isotopes are
323 preferentially released to the fluid phase at the onset of dissolution. This is because lighter
324 isotopes generally form weaker bonds that require less energy to break (see Oelkers et al.,
325 2015, 2018; Maher et al., 2016). Moreover, the transport of calcium, either through the fluid
326 or solid phase would favor the transfer to the fluid of light rather than heavy Ca. The second
327 mechanism, however, seems to be more likely as isotopic fractionation favors the
328 incorporation of light Ca into the calcite structure during its rapid precipitation (Lemarchand
329 *et al.*, 2004; Gussone *et al.*, 2005; Reynard *et al.*, 2011; Tang *et al.*, 2008, 2012). As such it
330 seems likely that the observed fractionation of Ca isotopes into the fluid phase during
331 congruent dissolution and at equilibrium stems from the two-way transfer of Ca between
332 calcite and the fluid phase. Such a process could proceed by the conservative release of Ca

333 from the calcite surface coupled to fractionation during its reincorporation into the solid
334 calcite. At bulk chemical equilibrium, this overall process would both maintain a constant
335 fluid Ca concentration and evolve the fluid-mineral system towards isotopic equilibrium. This
336 possibility is favored by the observation that the isotopic composition of the fluid phase
337 evolves after the fluid has attained bulk chemical equilibrium with the dissolving calcite (see
338 Figs 2 and 3). This possibility is also consistent with the concept of dynamic equilibrium (e.g.
339 Aagaard and Helgeson, 1982; Oelkers *et al.*, 1994; Schott and Oelkers, 1995; Oelkers, 2001;
340 Schott *et al.*, 2009, 2012; Steefel *et al.*, 2014; Lui *et al.* 2016). Note that a number of studies
341 have attempted to recover bulk mineral dissolution rates at close to equilibrium conditions
342 by measuring the temporal evolution of the isotopic composition of minerals and/or their
343 co-existing fluids (c.f. Gruber *et al.*, 2013; Zhu *et al.*, 2014; Subhas *et al.*, 2015, 2017; Liu *et*
344 *al.*, 2016; Naviaux *et al.*, 2019). It follows from the results presented in this study that such
345 efforts need to take explicit account of the role of mineral-fluid isotope exchange during
346 congruent dissolution and at bulk equilibrium to accurately retrieve near to equilibrium bulk
347 dissolution rates.

348 The observations of isotopic equilibration during the congruent dissolution and at
349 equilibrium in the present study differ fundamentally from the resetting of isotopic
350 compositions of biogenic carbonates as reported by Chanda *et al.* (2019). This former study
351 considered the temporal evolution of Ca isotope compositions in carbonate minerals that
352 contained substantial Mg in its structure placed in an initially Mg-free aqueous solution. This
353 resulted in the incongruent dissolution of the original biogenic carbonate, where the original
354 Mg bearing carbonate was replaced by a more stable Mg-poor calcite. The observed Ca
355 isotope composition evolution in the solids was thus driven by the thermodynamic instability
356 of the solids placed in the reactor. In contrast, the calcite in the present study dissolved

357 congruently and approached a stable bulk chemical equilibrium. Isotopic evolution in the
 358 experiments performed in the present study was thus driven by the isotopic disequilibrium
 359 in the water-mineral system.

360 Although the net mass of total calcium transferred from the calcite to the fluid phase
 361 via calcite dissolution is readily determined from the aqueous Ca concentrations (c.f. Fig 2b),
 362 it is challenging to estimate the fraction of the Ca in the original calcite transferred to the
 363 fluid and that reincorporated into the solid during each bulk reactor dissolution experiment.
 364 A crude estimate can be made by assuming that the Ca isotopic composition of the solid at
 365 the end of the dissolution experiments consisted of a fraction, f , of the Ca from the original
 366 bulk calcite and a fraction $1-f$ of Ca in isotopic equilibrium with the final fluid with a
 367 fractionation factor equal to $\Delta^{44/42}\text{Ca}_{\text{calcite-fluid}}$. Note such estimates do not take account of
 368 changing fluid compositions during water-mineral interaction, so tend to underestimate the
 369 overall mass of calcium exchanged. Taking account these assumptions and mass balance
 370 requires that

$$\begin{aligned}
 371 \quad & \delta^{44/42}\text{Ca}_{\text{final solid}} = \\
 372 \quad & f\delta^{44/42}\text{Ca}_{\text{initial solid}} + (1 - f)\delta^{44/42}\text{Ca}_{\text{final fluid}} - \Delta^{44/42}\text{Ca}_{\text{calcite-fluid}} \quad (4)
 \end{aligned}$$

373 The results of this calculation obtained from Eqn. (4) are shown in Fig 4 for the case of the
 374 dissolution leg of experiment A. In accord with these calculations, more than 90% of the Ca
 375 present in the original calcite powder would have equilibrated isotopically with the fluid
 376 phase during the dissolution leg of this experiment to attain the fluid phase $\delta^{44/42}\text{Ca}$
 377 observed at the end of the dissolution experiment for all $\Delta^{44/42}\text{Ca}_{\text{calcite-fluid}} < -0.9$ and more
 378 than 30% for all $\Delta^{44/42}\text{Ca}_{\text{calcite-fluid}} < -1.6$. The observed fluid phase $\delta^{44/42}\text{Ca}$ could not be
 379 attained with any $\Delta^{44/42}\text{Ca}_{\text{calcite-fluid}} < -0.82$. This comparison suggests that a majority of the

380 calcium present in the initial calcite grains were transferred into and out of the fluid phase
381 during the 8 to 9 day dissolution experiments performed in this study.

382 **4.2 Ca Isotope evolution during precipitation**

383 The variation of reactive fluid phase $\delta^{44/42}\text{Ca}$ as a function of time during the
384 precipitation leg of experiment A is similar to that predicted by Steefel et al. (2014) for the
385 precipitation of calcite in a closed system reactor. An initial stage of Ca isotope fractionation
386 is observed due to the kinetically controlled preferred incorporation of light Ca into the
387 precipitated calcite during the rapid precipitation of the mineral. This initial stage is followed
388 by a longer stage of isotopic re-equilibration. Within the Steefel et al. (2014) formalism, this
389 isotopic re-equilibration is a direct consequence of dynamic equilibrium; the combined
390 effects of reverse precipitation coupled to forward dissolution, which are equal at bulk
391 chemical equilibrium, tends to drive the mineral-fluid system towards isotopic equilibrium
392 after the calcite has precipitated.

393 Further insight into the evolution of the fluid phase calcium isotopic composition
394 during the calcite precipitation experiment can be gained with the aid of Fig. 5, which
395 compares the evolution of reactive fluid $\delta^{44/42}\text{Ca}$ as a function of F , the fraction of Ca
396 precipitated from the fluid during the experiment. The curves in this figure were calculated
397 assuming Rayleigh fractionation and equilibrium fraction (see Johnson *et al.*, 2004; Pearce *et*
398 *al.*, 2012) by assuming a calcite-fluid equilibrium fractionation factor of 0.4. Rayleigh
399 fractionation is consistent with the one-way transfer of material from the fluid phase into
400 the solid, whereas equilibrium fractionation requires the two-way transfer of material to and
401 from the precipitated solid. It can be seen that measured reactive fluid $\delta^{44}\text{Ca}$ is initially
402 consistent with Rayleigh fractionation, but that $\delta^{44/42}\text{Ca}$ evolves to become consistent with

403 equilibrium fractionation later in the experiment, while the calcite-reactive fluid system is at
404 chemical equilibrium within analytical uncertainty. This behavior is itself consistent with
405 kinetic theory; precipitation at far from equilibrium conditions is dominated by the transfer
406 of material from the fluid to the solid, whereas two way transfer dominates near and at
407 equilibrium in accord with the concept of dynamic equilibrium (e.g. Schott and Oelkers,
408 1995; Oelkers, 2001; Schott *et al.*, 2009; see also Pearce *et al.*, 2012).

409 An open question remains as the origin of the distinct behavior of calcium isotopic
410 transfer during dissolution and during precipitation in these experiments. The Ca isotope
411 fractionation during mineral precipitation was consistent with an equilibrium Ca
412 fractionation factor of ~ 0.4 , whereas that observed during calcite dissolution apparently
413 exceeds 0.8. One possible explanation for these contrasting equilibrium fractionation
414 factors is the distinct pH of the two experiments. The dissolution experiment presented in
415 this study was performed at pH 6.2, whereas the precipitation experiment was performed at
416 pH 7.5. Calcite dissolution rates are approximately 1.5 orders of magnitude faster at pH 6.2
417 compared to pH 7.5 (e.g. Chou *et al.*, 1989; Cubillis *et al.*, 2005). According to Tang *et al.*
418 (2008) this difference in reaction rates can more than double the Ca fractionation factor
419 between calcite and its co-existing aqueous fluid. The difference in pH of the fluid phase
420 however may also provoke a change in the Ca isotope fractionation due a change in aqueous
421 Ca speciation. The isotopic fractionation among aqueous species stems from the change in
422 coordination observed between aqueous Ca^{2+} and Ca-bearing complexes (see Moynier and
423 Fujii, 2017) and has been experimentally shown to be an important fractionation mechanism
424 for a number of divalent cations such as Mg and Zn (Schott *et al.*, 2016; Mavromatis *et al.*,
425 2019).

426 An alternative explanation for different observed fractionation factors in the different
427 experimental conditions is that the closed system experiments may not have completely
428 attained fluid-mineral isotopic equilibrium. Such uncertainties could be overcome through
429 the use of the three-isotope method to determine unambiguously both isotopic exchange
430 rates at bulk mineral fluid equilibrium as well as the equilibrium isotopic fractionation factor
431 in aqueous fluid-mineral systems (e.g. Beard *et al.*, 2010; Li *et al.*, 2011, 2014; Frierdich *et al.*,
432 2014; Reddy *et al.*, 2015; Zheng *et al.*, 2016; Stamm *et al.*, 2018).

433

434 **4.3 Preservation of isotopic signatures in natural systems**

435 The results reported in this study appear to contravene the commonly held
436 assumption that calcite can preserve its isotopic signatures over geological timeframes if
437 fluid-mineral isotopic disequilibrium exists, even if the fluid-mineral system is at bulk
438 chemical equilibrium. This observation is not unique to either calcite or the carbonate
439 minerals. Similar observations have been reported for the carbonates dolomite (Perez-
440 Fernandez *et al.*, 2017), hydromagnesite (Oelkers *et al.*, 2018) and other hydrous Mg-
441 carbonates (Mavromatis *et al.*, 2012, 2015), strontianite (Mavromatis *et al.*, 2017a), and
442 witherite (Mavromatis *et al.*, 2016), as well as non-carbonate minerals including goethite
443 (Beard *et al.*, 2010; Reddy *et al.*, 2015), epsomite (Li *et al.*, 2011), brucite (Li *et al.*, 2014),
444 quartz (Lui *et al.*, 2016), and amorphous SiO₂ (Stamm *et al.*, 2018). It follows that isotopic
445 preservation of the original Ca signature of calcite would require either the isolation of the
446 calcite-fluid system from external Ca input, by a process that decreases dramatically the rock
447 permeability or the slowing of the coupled mineral dissolution/precipitation reactions. There
448 is some indication that such processes are common in some natural systems. Turchyn and

449 DePaolo (2011) noted that much anecdotal evidence suggests that carbonate fossils are best
450 preserved in clay or organic-rich sedimentary horizons. The presence of clay minerals can
451 dramatically lower host rock permeability (e.g. Klimentos and McCann, 1990; Revel and
452 Cathels, 1999; Luijendijk and Gleeson, 2015) and thereby aid in the isolation of the fluid
453 system from external inputs. As a relatively small fraction of the Ca in most natural rocks is
454 present in the fluid phase, changes in fluid-mineral Ca isotopic fractionation due to
455 temperature changes would negligibly alter the isotopic signature of the calcite present in an
456 isolated system. Similarly, the presence of aqueous organic compounds may aid in the
457 preservation of isotopic compositions of calcite. Although they likely do not alter significantly
458 the dissolution rates of calcite (Oelkers *et al.*, 2011), the presence of aqueous organic
459 compounds can dramatically inhibit calcite precipitation (e.g. Meldrum and Hyde, 2001; de
460 Leeuw and Cooper, 2004; Lakshtnov *et al.*, 2011; Nielsen *et al.*, 2012; Mavromatis *et al.*,
461 2017c). As such it appears that Ca isotopic equilibration in the presence of aqueous organic
462 compounds may be slowed by a decrease in the rate of attachment of Ca to the calcite
463 surface. Moreover the presence of aqueous Mg has also been observed to slow calcite
464 precipitation rates (e.g. Fernandez-Diaz *et al.*, 1996; Morse *et al.*, 2007).

465 The results presented above suggest that isotopic exchange in calcite may be rapid
466 and stems from a coupled forward dissolution/reverse precipitation process. It seems likely,
467 therefore that the preservation of isotopic signals would be favored in minerals that have
468 relatively slow dissolution rates, or those that do not precipitate at ambient temperatures.
469 For the case of preserving calcium isotopic signals, apatite dissolves ~5 orders of magnitude
470 slower at ambient conditions and seawater pH (c.f. Plummer *et al.* 1979; Chou *et al.*, 1989;
471 Valsami-Jones *et al.*, 1998; Cubillis *et al.*, 2005; Chaïrat *et al.*, 2007). It therefore seems likely
472 that apatite may be a far better guardian of original Ca isotopic signatures than calcite. For

473 the case of carbonate minerals, dolomite or magnesite do not appear to precipitate via
474 abiotic processes at ambient temperatures (e.g. Saldi *et al.*, 2009, 2012; Gautier et al., 2014).
475 As such these minerals may better preserve original C and Mg and/or Ca isotopic signatures
476 than calcite.

477

478

5. Conclusions

479 The results of this study demonstrate isotopic compositions of calcite and its co-
480 existing fluid phase can be reset rapidly by congruent dissolution, precipitation, and at
481 equilibrium. As such the preservation of original Ca isotopic signatures in calcite may require
482 that the calcite is isotopically isolated from its surroundings, or a not yet to be identified
483 preservation mechanism is at play. Moreover, if the release of metals from minerals is
484 isotopically non-conservative as seems to be the case for calcite, it may not possible to use
485 the stable isotopic compositions of fluids to determine the source of metals, for example of
486 environmental pollutants. Such conclusions call for further investigation of the rates and
487 mechanisms of near to bulk equilibrium isotopic exchange to assess how best to interpret
488 the isotopic signals recorded in minerals and natural fluids.

489

490 Acknowledgements - We are grateful to Chen Zhu, Jacques Schott, Oleg Pokrovsky, Andrea
491 Perez-Fernandez, Nik Berninger, Franziska M. Stamm, Anna Harrison, Carl Steefel, Jenny
492 Druhan for encouragement and insightful discussion. We would also like to thank Alain
493 Castillo, Carol Causserand, and Thierry Aigouy for technical support. This study has been
494 supported by the Centre National de la Recherche Scientifique (CNRS), the European
495 Commission through Marie Cuire ITN projects MINSC (290040), METRANS (123456), and
496 CO2-REACT (317235). Isotopic analyses and PPvS were funded by NERC fellowship
497 NE/I020571/1.

498

499 **References**

- 500 Aagaard P. and Helgeson H.C. (1982) Thermodynamic and kinetic constraints on reaction-
501 rates among minerals and aqueous solutions. 1. Theoretical considerations. *Am. J. Sci.*
502 **282**, 237-285.
- 503 AlKhatib M. and Eisenhauer A. (2017) Calcium and strontium isotope fractionation in
504 aqueous solutions as a function of temperature and reaction rate: I. Calcite. *Geochim.*
505 *Cosmoshim. Acta* **209**, 298-319.
- 506 Beard B.L., Handler R.M., Scherer M.M., Wu L., Czaja A.D., Heimann A. and Johnson, C.M.
507 (2010) Iron isotope fractionation between aqueous ferrous iron and goethite. *Earth*
508 *Planet. Sci. Lett.* **295**, 241–250.
- 509 Blattler C.L., Jenkyns H.C., Reynard L.M. and Henderson G.M. (2011) Significant increases in
510 global weathering during Oceanic Anoxic Events 1A and 2 indicated by calcium isotopes.
511 *Earth Planet. Sci. Let.* **309**, 77-88.
- 512 Brunauer S., Emmett P, H., and Teller E. (1938) Adsorption of Gases in Multimolecular
513 Layers. *J. Am. Chem. Soc.* **60**, 309-319
- 514 Cenki-Tok B., Chabaux F., Lemarchand D., Schmidt A.D., Pierret M.C., Viville D., Bagard M.L.
515 and Stille, P. (2009) Then impact of water-rock interaction and vegetation on calcium
516 isotope fractionation in soil- and stream waters of a small forested catchment (the
517 Strengbach case). *Geochim Cosmochim. Acta* **73**, 2215-2228.
- 518 Chairat C., Schott J., Oelkers E. H., Lartigue J.-E. and Harouiya N. (2007) Kinetics and
519 mechanism of natural fluorapatite dissolution at 25 °C and pH from 3 to 12. *Geochim*
520 *Cosmochim Acta* **71**, 5901-5912.
- 521 Chanda, P., Gorski, C.A., Oakes, R.L., and Fantle, M. S., (2019) Low temperature stable
522 recrystallization of foraminifera tests and implications for the fidelity of geochemical
523 proxies. *Earth Planet Sci., Let.* **506**, 428-440.
- 524 Chou L., Garrels R.M. and Wollast, R. (1989) Comparative study of the kinetics and
525 mechanisms of dissolution of carbonate minerals. *Chem. Geol.* **78**, 269-282.
- 526 Chu N.-C., Henderson G.M., Belshaw N.S. and Hedges R.E.M. (2006) Establishing the
527 potential of Ca isotopes as proxy for consumption of dairy products. *App. Geochem.* **21**,
528 1656-1667.
- 529 Cubillas P., Köhler S.J., Prieto M., Chairat C. and Oelkers E.H. (2005) Experimental study of
530 the dissolution rates of calcite, aragonite, and bivalves. *Chem. Geol.* **216**, 59-77.
- 531 Curti E., Fujiwara K., Iijima K., Tits J., Cuesta C., Kitamura A., Glaus M.A. and Muller, W.
532 (2010) Radium uptake during barite recrystallisation at 23 ±Ra°C as a function of solution
533 composition: An experimental ¹³³Ba and ²²⁶Ra tracer study. *Geochim Cosmochim. Acta* **74**,
534 3553-3570.
- 535 De Leeuw N.H. and Cooper T.G. (2004) A computer modeling study of the inhibiting effect of
536 organic absorbates on calcite crystal growth. *Cryst. Growth Des.* **4**, 123-133.
- 537 DePaolo D.J. (2004) Calcium isotope variations produced by biological, radiogenic and
538 nucleosynthetic processes. *Rev. Min. Geochem.* **55**, 255-288.

- 539 Druhan J.L., Steefel C.I., Williams K.H. and DePaolo D.J. (2013) Calcium isotope fractionation
540 in groundwater: Molecular scale processes influencing field-scale behavior. *Geochim*
541 *Cosmochim. Acta* **119**, 93-116.
- 542 Fantle M.S. (2015) Calcium isotopic evidence for rapid recrystallization of bulk marine
543 carbonates and implications for geochemical proxies. *Geochim. Cosmochim. Acta* **148**
544 378-401.
- 545 Fantle M.S. and DePaolo D.J. (2007) Ca isotopes in carbonate sediment and pore fluid from
546 ODP Site 807A: the Ca²⁺(aq)-calcite equilibrium fractionation factor and calcite
547 recrystallization rates in Peistocene sediments. *Geochim. Cosmochim. Acta* **71**, 2524-
548 2546.
- 549 Fantle M.S. and Higgins J. (2014) The effects of diagenesis and dolomitiation on Ca and Mg
550 isotopes in marine platform carbonates: Implications for the global cycles of Ca and Mg.
551 *Geochim. Cosmochim. Acta* **142**, 458-481.
- 552 Fantle M.S., Maher K.M., and DePaolo D.J. (2010) Ca isotopic approaches for quantifying
553 rates of marine burial diagenesis. *Rev. Geophys.* **48**, RG302.
- 554 Fantle M.S. and Tipper E.T. (2014) Calcium isotopes in the global biogeochemical Ca cycle:
555 Implications for development of a Ca isotope proxy. *Earth. Sci. Rev.* **129**, 148-177.
- 556 Fairchild I.J., Smith C.L., Baker A., Fuller L., Spotl C., Matthey D. and McDermott F. (2006)
557 Modification and preservation of environmental signals in speleotherms. *Earth-Sci.*
558 *Revs.* **75**, 105-153.
- 559 Farkas J., Fryda J. and Holden C. (2016) Calcium isotope constraints on the marine carbon
560 cycle and CaCO₃ deposition during the Silurian (Ludfordian) positive delta ¹³C excursion.
561 *Earth Planet Sci Let.* **451**, 31-40.
- 562 Fernandez-Diaz L., Putnis A., Prieto M., Putnis C.V. (1996) The role of magnesium in the
563 crystallization of calcite and aragonite in a porous medium. *J. Sed. Res.* **66**, 482-491.
- 564 Frierdich A.J., Beard B.L., Scherer M.M. and Johnson, C.M. (2014) Determination of the
565 Fe(II)aq–magnetite equilibrium iron isotope fractionation factor using the three-isotope
566 method and a multi-direction approach to equilibrium. *Earth Planet. Sci. Lett.* **391**, 77–
567 86.
- 568 Gautier, Q., Bénézech, P., Mavromatis, V., Schott, J., 2014. Hydromagnesite solubility product
569 and growth kinetics in aqueous solution from 25 to 75°C. *Geochim. Cosmochim. Acta*
570 **138**, 1-20.
- 571 Grazis C. and Feng X.H. (2004) A stable isotope study of soil water: Evidence for mixing and
572 preferential flow paths. *Geoderma* **119**, 97-111.
- 573 Gruber C., Harpaz L., Zhu C., Bullen T.D. and Ganor J. (2013) A new approach for measuring
574 dissolution rates of silicate minerals by using silicon isotopes. *Geochim. Cosmochim.*
575 *Acta* **104**, 261-280.
- 576 Gussone N., Bohm F., Eisenhaur A., Dietzel M., Heuser A., Teichert B.M.A., Reitner J.,
577 Worheide G. and Dullo W.C. (2005) Calcium isotope fractionation in calcite and
578 aragonite. *Geochim. Cosmochim. Acta* **69**, 4485-4494.

- 579 Gussone N. Nehrke G. and Teichert B.M.A. (2011) Calcium isotope fractionation in ikaite and
580 vaterite. *Chem. Geol.* **285**, 194-202.
- 581 Harouaka K., Eisenhauer A. and Fantle M.S. (2014) Experimental investigation of Ca isotope
582 fractionation during abiotic gypsum precipitation. *Geochim. Cosmochim. Acta* **129**, 157-
583 176.
- 584 Heuser A., Eisenhauer A., Bohm F., Wallmann K., Gussone N., Pearson P.N., Nagler T.F. and
585 Dullo W.C. (2005) Calcium, isotope (δ Ca-44/40) variations of Neogene planktonic
586 foraminifer. *Paleoceanography* **20**, DOI: 10.1029/2004PA001048.
- 587 Hindshaw R.S., Bourdon B., Pogge von Strandmann P., Vigier N., and Burton K., (2013) The
588 stable calcium isotopic composition of rivers draining basaltic catchments in Iceland.
589 *Earth Planet. Sci. Let.* **374**, 173-184.
- 590 Hindshaw R.S., Reynolds B.C., Wiederhold J.G., Kretzschmar R., and Bourdon B. (2011)
591 Calcium isotopes in a proglacial weathering environment: Damma Glacier, Switzerland.
592 *Geochim. Cosmochim. Acta* **75**, 106-118.
- 593 Holmden C. and Belanger N. (2010) Ca isotope cycling in a forested catchment. *Geochim.*
594 *Cosmochim. Acta* **74**, 995-1015.
- 595 Jacobson A.D. and Holmden C. (2008) Δ -⁴⁴Ca evolution in a carbonate aquifer and its
596 bearing on the equilibrium isotope fractionation factor for calcite. *Earth. Planet. Sci. Let.*
597 **270**, 349-353.
- 598 Johnson C.M., Beard B.L. and Albarede F. (2004) Overview and General Concepts. *Rev. Min.*
599 *Geochem.* **55**, 1-24.
- 600 Jost A.B., Mundil R., He B., Brown S. T., Altiner D., Sun Y., DePaolo D.J. and Payne J.L. (2014)
601 Constraining the cause of the end-Guadalupean extinction with coupled records of
602 carbon and calcium isotopes. *Earth Planet. Sci. Let.* **396**, 201-212.
- 603 Kasemann, S.A. Hawkesworth C.J., Prave A.R., Fallick A.E. and Person P.N. (2005) Boron and
604 calcium isotopic composition in Neoproterozoic carbonate rocks from Namibia:
605 Evidence for extreme environmental change. *Earth Planet. Sci. Let.* **231**, 73-86.
- 606 Kasemann S.A., Pogge von Strandmann P.A.E., Prave A. R., Fallick A.E., Elliott T. and
607 Hoffmann K-H. (2014) Continental weathering following a Cryogenian glaciation:
608 Evidence from calcium and magnesium isotopes. *Earth Planet. Sci. Let.* **396**, 66-77.
- 609 Klimentos, T. and McCann C. (1990) Relationships among compressional wave attenuation,
610 porosity, clay content, and permeability in sandstones. *Geophys.* **55**, 998-1014.
- 611 Koch P. L. (1998) Isotopic reconstruction of past continental environments. *Ann. Rev. Earth*
612 *Planet. Sci.* **26**, 573-613.
- 613 Lakshtnov L.Z., Bovet N. and Stipp, S.L.S. (2011) Inhibition of calcite growth by alginate.
614 *Geochim. Cosmochim. Acta* **75**, 3945-3955.
- 615 Lemarchand D., Wasserburg G. and Papanastassiou D. (2004) Rate-controlled calcium
616 isotope fractionation in synthetic calcite. *Geochim. Cosmochim. Acta* **68**, 4665-4678.
- 617 Leng M. J. and Marshall J. D. (2004) Palaeoclimate interpretation of stable isotope data from
618 lake sediment archives. *Quarter. Sci. Revs.* **23**, 811-831.

- 619 Li W., Beard B.L. and Johnson C.M. (2011) Exchange and fractionation of Mg isotopes
620 between epsomite and saturated MgSO₄ solution. *Geochim. Cosmochim. Acta* **75**, 1814–
621 1828.
- 622 Li W., Beard B.L., Li C. and Johnson, C.M. (2014) Magnesium isotope fractionation between
623 brucite [Mg(OH)₂] and Mg aqueous species: Implications for silicate weathering and
624 biogeochemical processes. *Earth Planet. Sci. Lett.* **394**, 82–93.
- 625 Li X., DePaolo D.J., Wang Y.X. and Xie X.J. (2018) Calcium isotope fractionation in a silicate
626 dominated Cenozoic aquifer system. *J. Hydrology* **229**, 523-533.
- 627 Liu, Z., Rimstidt, J.D., Zhang, Y., Yuan, H., and Zhu, C. (2016) A stable isotope doping method
628 to test the range of applicability of detailed balance. *Geochem. Perspective Lett.* **2**, 78-
629 86.
- 630 Luijendijk E. and Gleeson T. (2015) How well can we predict permeability in sedimentary
631 basins? Deriving and evaluating porosity-permeability equations for non-cemented sand
632 and clay mixtures. *Geofluids* **15**, 67-83.
- 633 Lyons W.B., Bullen T.D. and Welch K.A. (2017) Ca isotopic geochemistry of an Antarctic
634 aquatic system. *Geophys. Res. Lett.* **44**, 882-891.
- 635 Maher, K., Johnson, N.C., Jackson, A., Lammers, L.N., Torchinsky, A.B., Weaver, K.L., Bird,
636 D.K., Brown, G.E., 2016. A spatially resolved surface kinetic model for forsterite
637 dissolution. *Geochim. Cosmochim. Acta* **174**, 313-334.
- 638 Marriott C. S., Henderson G. M., Belshaw N. S. and Tudhope A. W. (2004) Temperature
639 dependence of $\delta^7\text{Li}$, $\delta^{44}\text{Ca}$ and Li/Ca during growth of calcium carbonate. *Earth. Planet.*
640 *Sci. Lett.* **222**, 615-624.
- 641 Marshall J.D. (1992) Climate and oceanographic isotopic signals from the carbonate rock
642 record and their preservation. *Geol. Mag.*, **129**, 143-160.
- 643 Mavromatis V., Pearce C. R., Shirokova L. S., Bundeleva I. A., Pokrovsky O. S., Benezeth P. and
644 Oelkers E. H. (2012) Magnesium isotope fractionation during hydrous magnesium
645 carbonate precipitation with and without cyanobacteria. *Geochim. Cosmochim. Acta* **76**,
646 161-174.
- 647 Mavromatis V., Bundeleva I.A., Shirokova L.S., Millo C., Pokrovsky O.S., Benezeth P., Ader M.
648 and Oelkers E.H. (2015) The rapid resetting of carbon isotope signatures of hydrous Mg
649 carbonate in the presence of cyanobacteria. *Chem. Geo.* **404**, 41-51.
- 650 Mavromatis V., van Zuilen, K., Purgstaller, B., Baldermann, A., Nagler, T.F. and Dietzel, M.
651 (2016) Barium isotope fractionation during witherite (BaCO₃) dissolution, precipitation
652 and at equilibrium. *Geochim. Cosmochim. Acta* **190**, 72-84.
- 653 Mavromatis V., Harrison A. L., Eisenhauer A. and Dietzel, M. (2017a). Strontium isotope
654 fractionation during strontianite (SrCO₃) dissolution, precipitation and at equilibrium.
655 *Geochim. Cosmochim. Acta* **218**, 201-214.
- 656 Mavromatis V., Purgstaller B., Dietzel M., Buhl D., Immenhauser A. and Schott J. (2017b)
657 Impact of amorphous precursor phases on magnesium isotope signatures of Mg-calcite.
658 *Earth Planet. Sci. Lett.* **464**, 227–236.

659 Mavromatis, V., Gonzalez, A.G., Dietzel, M., and Schott, J. (2019) Zinc isotope fractionation
660 during the inorganic precipitation of calcite - Towards a new pH proxy. *Geochim.*
661 *Cosmochim. Acta* **244**, 99-112.

662 Mavromatis, V., Immenhauser, A., Buhl, D., Purgstaller, B., Baldermann, A., and Dietzel, M.
663 (2017c) Effect of organic ligands on Mg partitioning and Mg isotope fractionation during
664 low-temperature precipitation of calcite in the absence of growth rate effects. *Geochim.*
665 *Cosmochim. Acta* **207**, 139-153.

666 Meldrum F.C., and Hyde S.T. (2001) Morphological influence of magnesium and organic
667 additives on the precipitation of calcite. *J. Cryst. Growth* **231**, 554-558.

668 Morse J.W., Arvidson R.S., Luttge A. (2007) Calcium carbonate formation and dissolution.
669 *Chem. Rev.* **107**, 342-381.

670 Moynier, F., and Fujii, T. (2017) Calcium isotope fractionation between aqueous compounds
671 relevant to low-temperature geochemistry, biology and medicine. *Sci Rep* **7**.

672 Nagler T.S., Eisenhauer A., Muller A., Hemleben C., and Kramers J. (2000) The $\delta^{44}\text{Ca}$ -
673 temperature calibration on fossil and cultured *Globigernoides sacculifer*: new tool for
674 reconstruction of past sea surface temperatures, *Geochem. Geophys. Geosyst.*
675 12000GC000091.

676 Naviaux, J.D., Subhas, A.V., Rollins, N.E., Dong, S., Berelson. W.M. and Adkins, J.F. (2019)
677 Temperature dependence of calcite dissolution in seawater. *Geochim. Cosmochim. Acta*
678 **246**, 363-384.

679 Neilsen J.W., Sand K.K., Pedersen C.S., Lakshatanov L.Z., Winther J.R., Willemoes M. and Stipp,
680 S.L.S. (2013) Polysaccharide effects in calcite growth: The influence of composition and
681 branching. *Crystal Growth Des.* **12**, 4906-4910.

682 Oelkers E. H. (2001) General kinetic description of multioxide silicate mineral and glass
683 dissolution. *Geochim. Cosmochim. Acta* **65**, 3703-3719.

684 Oelkers E. H., Schott J. and Devidal J.-L. (1994) The effect of aluminum, pH, and chemical
685 affinity on the rates of aluminosilicate dissolution reactions. *Geochim. Cosmochim.*
686 *Acta* **58**, 2011-2024.

687 Oelkers E.H., Golubev S.V., Pokrovsky O.S. and Benezeth P. (2011) Do organic ligands affect
688 calcite dissolution rates? *Geochim. Cosmochim. Acta* **75**, 1799-1813.

689 Oelkers, E.H., Benning, L.G., Lutz, S., Mavromatis, V., Pearce, C.R., Plümper, O., 2015. The
690 efficient long-term inhibition of forsterite dissolution by common soil bacteria and fungi
691 at Earth surface conditions. *Geochim. Cosmochim. Acta* **168**, 222-235.

692 Oelkers E.H., Berninger U.-N., Perez-Fernandez A., Chmeleff J. and Mavromatis V. (2018) The
693 temporal evolution of magnesium isotope fractionation during hydromagnesite
694 dissolution, precipitation, and at equilibrium. *Geochim. Cosmochim. Acta* **226**, 36-49.

695 Owen R.A., Day C.C., Hu C.-Y., Lui Y.H., Pointing M.D., Blaettler, C.L. and Henderson, G.M.
696 (2016) Calcium isotopes in caves as a proxy for aridity: Modern calibration and
697 application to the 8.2 kyr event. *Earth Planet. Sci. Let.* **442**, 129-138.

698 Page B.D., Bullen T.D. and Mitchell M.J. (2008) Influences of calcium availability and tree
699 species on Ca isotope fractionation in soil and vegetation. *Biogeochem.* **88**, 1-13.

- 700 Parkhurst D. L. and Appelo C. A. J. (1999) User's Guide to PHREEQC (Version 2) – A Computer
701 Program for Speciation, Batch- Reaction, One-Dimensional Transport, and Inverse
702 Geochemical Calculations. U.S. Geological Survey Water-Resources Investigations Report
703 99-4259, 310pp.
- 704 Pearce C. R., Saldi G. D., Schott J. and Oelkers E. H. (2012) Isotopic fractionation during
705 congruent dissolution, precipitation and at equilibrium: Evidence from Mg isotopes.
706 *Geochim. Cosmochim. Acta* **92**, 170-183.
- 707 Perez-Fernandez A., Berninger, U.-N. Mavromatis V., Pogge Von Strandmann, P.A.E. and
708 Oelkers E.H. (2017) Ca and Mg isotope fractionation during the stoichiometric dissolution
709 of dolomite at 51 to 126 °C and 5 bars CO₂ pressure. *Chem. Geol.* **467**, 76-88.
- 710 Plummer L.N., Wigley T.M.L. and Parkhurst D.L. (1979) Critical review of the kinetics of
711 calcite dissolution and precipitation. *in*: Jeune, E.A., ed., Chemical modeling in aqueous
712 systems: American Chemical Society Symposium Series 93:537-573.
- 713 Pruss S.B., Blatter C.L., MacDonald F.A. and Higgins J.A. (2018) Calcium isotope evidence that
714 the earliest metazoan biomineralizers forms aragonite shells. *Geology* **46**, 736-766.
- 715 Reddy T.R., Friedrich A.J., Beard B.L. and Johnson, C.M. (2015) The effect of pH on stable iron
716 isotope exchange and fractionation between aqueous Fe(II) and goethite. *Chem. Geol.*
717 **397**, 118–127.
- 718 Revel A. and Cathels L.M. (1999) Permeability of shaly sands. *Water Resour. Res.* **35**, 651-662.
- 719 Reynard L.M., Day C.C. and Henderson G.M. (2011) Large fractionation of calcium isotopes
720 during cave-analogue calcium carbonate growth. *Geochim. Cosmochim. Acta* **75**, 3726-
721 3740.
- 722 Reynard L.M., Henderson G.M. and Hedges, R.E.M. (2010) Calcium isotope ratios in animal
723 and human bone. Large fractionation of calcium isotopes during cave-analogue calcium
724 carbonate growth. *Geochim. Cosmochim. Acta* **74**, 3735-3750.
- 725 Ryu J.S., Jacobsen A.D., Holmden C., Lundstrom, C. and Zhang, Z.F. (2011) The major ion,
726 $\delta^{44/40}\text{Ca}$, $\delta^{44/42}\text{Ca}$ and $\delta^{26/24}\text{Mg}$ geochemistry of granite weathering at pH=1 and T=25 C:
727 Power law processes and the relative reactivity of minerals. *Geochim. Cosmochim. Acta*
728 **75**, 6004-6026.
- 729 Saldi G.D., Jordan G., Schott, J. and Oelkers E.H. (2009) Magnesite growth rates as a function
730 of temperature and saturation state. *Geochim. Cosmochim. Acta.* **73**, 5646-5657.
- 731 Saldi G.D., Schott J., Pokrovsky O.S., Gautier Q. and Oelkers E.H. (2012) An experimental
732 study of magnesite precipitation rates at neutral to alkaline conditions and 100 to 200 °C
733 as a function of pH, aqueous solution composition and chemical affinity *Geochim.*
734 *Cosmochim. Acta*, **83**, 93-109.
- 735 Sawaki Y., Tahata M., Ohno T., Komiya T., Hirata T., Maruyama S., Han, J. and Shu D. (2014)
736 The anomalous Ca cycle in the Ediacaran ocean: Evidence from Ca isotopes preserved in
737 the Three Gorges area, South China. *Gondwana Res.* **25**, 1070-1089.
- 738 Shirokova L.S., Mavromatis V., Bundeleva I.A., Pokrovsky O.S., Benezeth P., Gerard E., Pearce
739 C.R. and Oelkers E.H. (2013) Using Mg isotopes to trace cyanobacterially mediated
740 magnesium carbonate precipitation in alkaline lakes. *Aquat. Geochem.* **19**, 1-24.

- 741 Schmitt A.D., Bracke G., Stille P. and Kierel B. (2001) The calcium isotope composition of
742 modern seawater determined by thermal ionisation mass spectrometry. *Geostandards*
743 *Newsletter* **25**, 1-9.
- 744 Schott J. and Oelkers E. H. (1995) Dissolution and crystallization rates of silicate minerals as a
745 function of chemical affinity. *Pure App. Chem.* **67**, 903-910.
- 746 Schott J., Pokrovsky O. S. and Oelkers E. H. (2009) The link between mineral
747 dissolution/precipitation kinetics and solution chemistry. *Rev. Min. Geochem.* **70**, 207-
748 258.
- 749 Schott J., Pokrovsky O. S. Benezeth P., Goderris Y. and Oelkers E. H. (2012) Can accurate rate
750 laws be created to describe chemical weathering? *Comptes Rendus Geosci.* **344**, 568-
751 585.
- 752 Schott, J., Mavromatis, V., Fujii, T., Pearce, C.R., Oelkers, E.H., 2016. The control of carbonate
753 mineral Mg isotope composition by aqueous speciation: Theoretical and experimental
754 modeling. *Chem. Geol.* **445**, 120-134.
- 755 Silva-Tamayo J.C., Lau K.V., Jost A.B., Payne J.L., Wignall P.B., Newton R.J., Eisenhauer A.,
756 DePaolo D.J., Brown S., Maher K., Lehrmann D.J., Altiner D., Yu M.Y., Richoz S. and
757 Paytan A. (2018) Global perturbation of the marine calcium cycle during the Permian-
758 Triassic transition. *Geol. Soc. Am. Bull.* **130**, 1323-1338.
- 759 Stamm F.M., Zambardi T., Chmeleff J., Schott J., von Blanckenburg F. and Oelkers E.H. (2018)
760 The experimental determination of equilibrium Si isotope fractionation factors among
761 $\text{H}_4\text{SiO}_4^\circ$, H_3SiO_4^- and amorphous silica ($\text{SiO}_2 \cdot 0.32 \text{H}_2\text{O}$) at 25 and 75°C using the three
762 isotope method. *Geochim. Cosmochim. Acta* submitted.
- 763 Steefel C.I., Druham J.L. and Maher, K. (2014) Modelled coupled chemical and isotopic
764 equilibration rates. *Proced. Earth Planet. Sci.* **10**, 208-217.
- 765 Subhas, A.V., Rollins, N.E., Berelson, W.M., Dong, S., Erez, J. and Adkins, J.F. (2015) A novel
766 determination of calcite dissolution kinetics in seawater. *Geochim. Cosmochim. Acta*
767 **170**, 52-68.
- 768 Subhas, A.V., Adkins, J.F., Rollins, N.E., Naviaux, J., Erez, J., and Berelson, W.M. (2017)
769 Catalysis and chemical mechanism of calcite dissolution in seawater. *Proc. Nat. Acad. Sci.*
770 **114**, 8175-8180.
- 771 Tang J., Dietzel M., Böhm F., Köhler S.J. and Eisenhauer A. (2008) $\text{Sr}^{2+}/\text{Ca}^{2+}$ and $^{44}\text{Ca}/^{40}\text{Ca}$
772 fractionation during inorganic calcite formation: II. Ca isotopes. *Geochim. Cosmochim.*
773 *Acta* **72**, 3733-3745.
- 774 Tang J., Niedermayr A., Köhler S.J., Bohm F., Kiskurek B., Eisenhauer A. and Dietzel M.
775 (2012) $\text{Sr}^{2+}/\text{Ca}^{2+}$ and $^{44}\text{Ca}/^{40}\text{Ca}$ fractionation during inorganic calcite formation: III.
776 Impact of salinity.ionic strength. *Geochim Cosmochim. Acta* **77**, 432-443.
- 777 Teichert B.M.A., Gussone N. and Torres, M.E. (2009) Controls on calcium isotope
778 fractionation in sedimentary porewaters. *Earth Planet. Sci. Let.* **279**, 373-382.

- 779 Tipper E.T., Galy A. and Bickle M.J. (2006) Riverine evidence for a fractionated reservoir of Ca
780 and Mg on the continents: Implications for the oceanic Ca cycle. *Earth Planet. Sci. Let.*
781 **247**, 267-279.
- 782 Tipper E.T., Galy A. and Bickle M.J. (2008) Calcium and magnesium isotope systematics in
783 rivers draining the Himalaya-Tibetan plateau region: Lithological or fractionation control?
784 *Geochim Cosmochim Acta* **72**, 1057-1075.
- 785 Turchyn A.V. and DePaolo D.J. (2011) Calcium isotope evidence for suppression of carbonate
786 dissolution in carbonate-bearing organic-rich sediments. *Geochim. Cosmochim. Acta* **75**,
787 7081-7098.
- 788 Valsami-Jones E., Ragnarsdottir K.V., Putnis A., Bosbach D., Kemp A.J. and Cressey, G., (1998)
789 The dissolution of apatite in the presence of aqueous metal cations at pH 2-7. *Chem.*
790 *Geo.* **151**, 215-233.
- 791 Van't Hoff, M.J.H. (1884) Etudes de dynamique chimique. *Recueil Travaux Chimiques Pas-Bas*
792 **3**, 333-336.
- 793 Voigt M., Marieni C., Clark D.E., Gislason, S.R. and Oelkers E.H. (2018) Evaluation and
794 refinement of thermodynamic databases for mineral carbonation. *Energy Procedia* **146**,
795 81-91.
- 796 Wang W.Z., Qin T., Zhou C., Huang S.C. Wu Z.Q. and Huang F. (2017) Concentration effect on
797 equilibrium fractionation of Mg-Ca isotopes in carbonate minerals. Insights from first
798 principle calculations. *Geochim. Cosmochim. Acta* **208**, 185-197.
- 799 Wiederhold J.G. (2015) Metal isotope signatures as tracers in environmental geochemistry.
800 *Envir. Sci. Tech.* **49**, 2606-2624.
- 801 Yan H., Schmitt A.D., Liu Z.H. Gangloff S., Sun H.L., Chen J.B. and Chabaux F. (2016) Calcium
802 isotopic fractionation during travertine deposition under different conditions: Examples
803 from Baishuitai (Yunan, SW China). *Chem. Geol.* **426**, 60-70.
- 804 Zheng X.-Y., Beard B.L., Reddy T.R., Roden E.E. and Johnson C.M. (2016) Abiologic silicon
805 isotope fractionation between aqueous Si and Fe(III)-Si gel in simulated Archean
806 seawater: Implications for Si isotope records in Precambrian sedimentary rocks.
807 *Geochim. Cosmochim. Acta* **187**, 102-122.
- 808 Zhu C., Liu Z.Y., Schaefer A., Wang C., Zhang G.R., Gruber C., Ganor J. and Gerog R.B. (2014)
809 Silicon isotopes as a new method of measuring silicate mineral reaction rates at ambient
810 temperature. *Proc. Earth Planet. Sci.* **10**, 189-193.
- 811 Zhu P. and Macdougall J.D. (1998) Calcium isotopes in the marine environment and the
812 oceanic calcium cycle. *Geochim. Cosmochim. Acta* **62**, 1691-1698.

813

814 **Figure Captions**

815 Figure 1. SEM images of the calcite powder used in the experiments a) the initial calcite prior
816 to experiment A, b) the calcite grains recovered after the experiment A, and c) calcite
817 grains recovered after experiment B.

818

819 Figure 2: Temporal chemical and isotopic evolution of the fluid phase during experiment A:
820 a) Measured fluid phase Ca concentration, the error bars in this figure correspond to an
821 estimated 4% uncertainty in these analyses; b) fraction of the total Ca preset in the
822 system within calcite, the error bars in this plot represent an estimated 2% uncertainty in
823 these values; c) fluid Ca isotopic composition; the error bars in c are taken as two
824 standard deviations of repeated analyses. Note that the pH of the fluid phase was
825 changed after 25 and after 125 hours, by changing the identity of the gas bubbling
826 through the reactor. The timing of these pH changes is indicated by the vertical lines. The
827 thin dashed curves in a were calculated using calcite dissolution/precipitation rate
828 equations of Chou et al. (1989) whereas those in b and c are for the aid of the reader.
829 The thick dashed line in c corresponds to the Ca isotopic composition of the original
830 dissolving solid its associated 2 standard deviation uncertainty – see text and Table1.

831

832 Figure 3: Temporal chemical and isotopic evolution of the fluid phase during experiment B:
833 a) Measured fluid phase Ca concentration, the estimated 4% uncertainty in these
834 analyses is within the size of their symbol; b) fluid Ca isotopic composition; the error bars
835 in b are taken as two standard deviations of repeated analyses. The dashed curve in a
836 were calculated using calcite dissolution/precipitation rate equations of Chou et al.
837 (1989) whereas that in b is for the aid of the reader. The thick grey line in c corresponds
838 to the Ca isotopic composition of the original dissolving solid and its associated 2
839 standard deviation uncertainty – see text and Table1.

840

841 Figure 4. Calculated fraction of calcite present in the initial calcite (f) required to pass through
842 the fluid phase to obtain the observed fluid phase Ca isotopic composition at the end of
843 the dissolution leg of Experiment A, as a function of the equilibrium calcite-fluid Ca
844 fractionation factor.

845

846 Figure 5: The Ca isotopic composition of the fluid phase provoked by calcite precipitation
847 during the final 240 hours of experiment A plotted as a function of the fraction of the
848 reactive fluid Ca incorporated into the solid. The solid curve represents the fluid
849 composition of this fluid calculated using a Rayleigh distillation model whereas the linear
850 curve corresponds to the fluid composition calculated with an equilibrium fractionation
851 model. In each case the solid curves were calculated by adopting the calcium-fluid
852 fractionation factor, $\Delta^{44/42}\text{Ca}_{\text{fluid-solid}} = -0.4$.

853

854

855

856

857 Table 1. Measured chemical and isotopic composition of the fluid and solid phases during
 858 experiment A. Note that the pH of the fluid phase was changed after 25 and 218 hours of
 859 elapsed time by changing the composition of the gas bubbled through the reactor – see text.
 860

Sample	Elapsed time (hours)	Reactive fluid mass (g) ^a	pH	C _{Ca} (mol/kg x10 ³)	Alkalinity (eq/kg x10 ³)	Percent aqueous Ca ^b	δ ^{44/42} Ca ^c	Saturation index ^d
A-1	25	948.2	8.39	0.22	5	0.9	0.01±0.03	0.24
A-2	48	933.3	6.23	3.85	29	15.6	0.28±0.11	-0.02
A-3	73	918.3	6.23	4.99	33	20.1	0.34±0.06	0.10
A-4	96	902.4	6.19	4.14	32	16.8	0.36±0.07	-0.02
A-5	145	886.6	6.19	4.21	32	17.0	0.55±0.04	-0.02
A-6	170	870.7	6.20	4.80	33	19.3	0.27±0.04	0.05
A-7	196	854.4	6.18	4.99	36	20.0	0.51±0.12	0.07
A-8	218	837.6	6.18	4.81	35	19.3	0.57±0.01	0.05
A-9	242	810.0	7.43	1.65	3.8	8.0	0.72±0.07	0.08
A-10	265	780.7	7.49	1.75	2.7	8.4	1.06±0.06	0.02
A-11	289	751.6	7.56	1.75	2.7	8.4	1.15±0.04	0.09
A-12	337	722.4	7.46	1.94	2.8	9.0	0.75±0.09	0.05
A-13	363	692.4	7.48	1.81	2.8	8.6	0.77±0.01	0.04
A-14	385	660.9	7.49	1.87	2.4	8.7	0.92±0.04	0.00
Initial Calcite							-0.25±0.08	
Final Calcite							-0.41±0.01	

861

862

863 a) Reactive fluid remaining in the reactor after the fluid sample was collected as determined by
 864 weighing the fluid samples. b) Percent of calcium in the batch reactor present in the aqueous phase
 865 as calculated from mass balance constraints. c) All δ^{44/42}Ca listed in this table were measured; listed
 866 +/- uncertainties refer to two standard deviations of repeated analyses. d) Saturation index of the
 867 sampled aqueous fluid with respect to calcite calculated using the PHREEQC computer code
 868 together with its minteq.v4 database. It is estimated that the uncertainty in calculated saturation
 869 indexes are approximately ±0.1.
 870

871
872
873
874

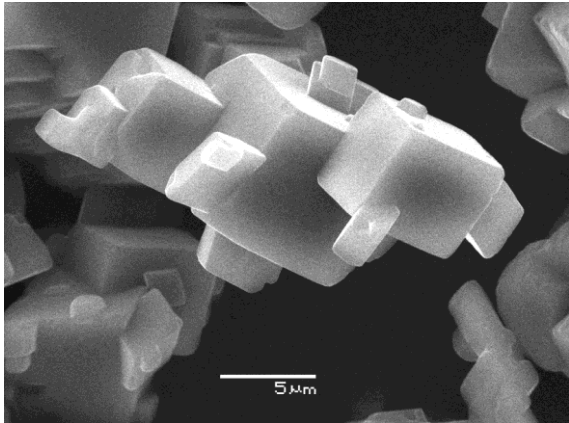
Table 2. The measured chemical and isotopic composition of the fluid and solid phases during experiment B.

Sample	Elapsed time (hours)	Reactive fluid mass (g) ^a	<i>pH</i>	<i>C</i> _{Ca} (mol/kg x10 ³)	Alkalinity (eq/kg x10 ³)	Percent Aqueous Ca ^b	$\delta^{44/42}\text{Ca}^c$	Saturation index ^d
B-1	3	984.7	6.39	8.77	8.32	43.2	0.15±0.08	-0.01
B-2	5.5	965.7	6.21	9.31	11.49	45.9	0.22±0.06	-0.05
B-3	28	947.6	6.28	9.27	11.13	45.7	0.45±0.05	0.01
B-4	45	927.5	6.23	9.40	11.26	46.3	0.42±0.02	-0.03
B-5	70	909.3	6.25	9.42	11.24	46.4	0.50±0.04	-0.01
B-6	101	891.4	6.23	9.44	10.74	46.5	0.52±0.10	-0.03
B-7	121	875.7	6.22	9.46	11.02	46.6	0.64±0.10	-0.05
B-8	149	858.0	6.25	9.64	11.04	47.3	0.59±0.04	-0.01
B-9	172	838.5	6.25	9.66	12.03	47.4	0.52±0.03	0.02
B-10	193	814.2	6.26	9.09	10.64	45.1	0.64±0.04	-0.04
Initial Calcite							0.12±0.07	
Final Calcite							-0.07±0.02	

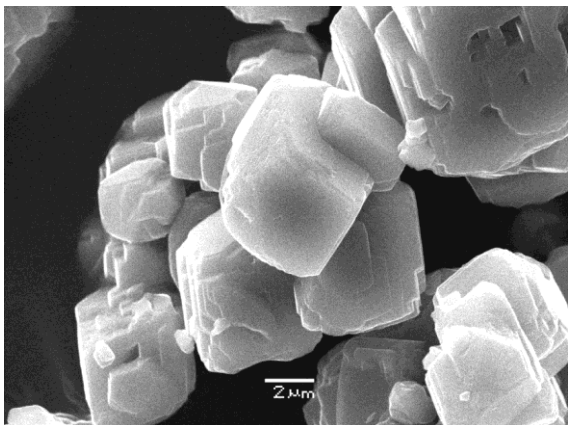
875
876
877
878
879
880
881
882
883
884
885
886
887

a) Reactive fluid remaining in the reactor after the fluid sample was collected as determined by weighing the fluid samples. b) Percent of calcium in the batch reactor present in the aqueous phase as calculated from mass balance constraints. c) All $\delta^{44/42}\text{Ca}$ listed in this table were measured; listed +/- uncertainties refer to two standard deviations of repeated analyses. d) Saturation index of the sampled aqueous fluid with respect to calcite calculated using the PHREEQC computer code together with its minteq.v4 database. It is estimated that the uncertainty in calculated saturation indexes are approximately ±0.1.

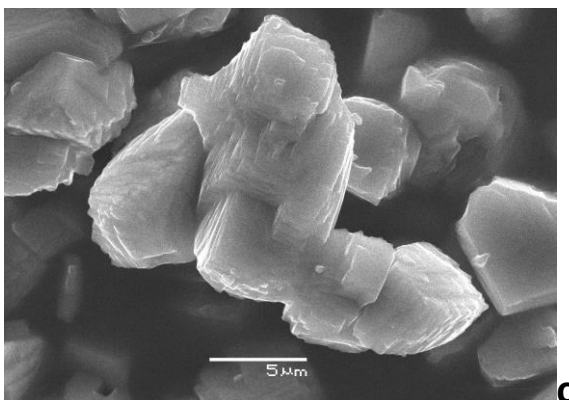
888



a.



b.



c.

889

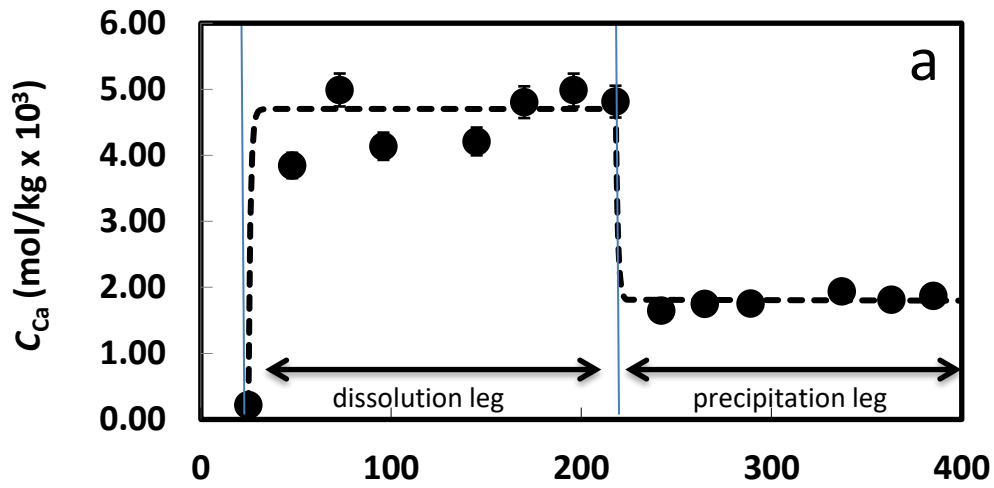
890

891

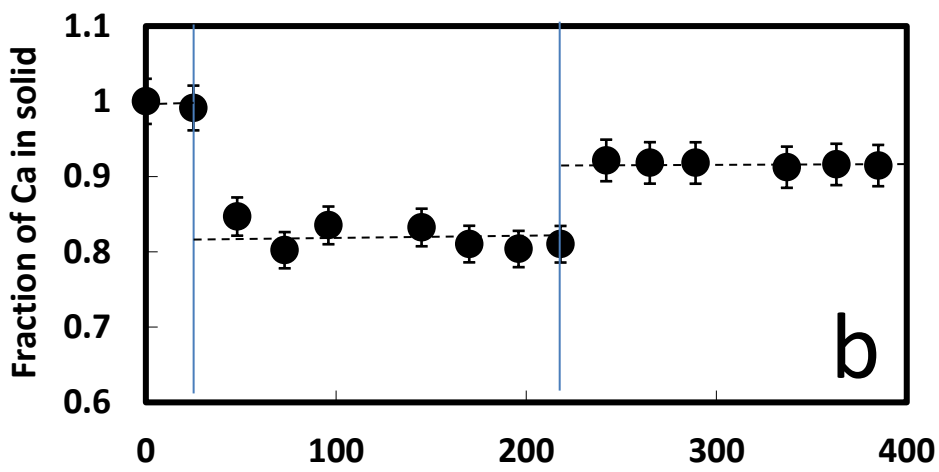
892 **Figure 1.**

893

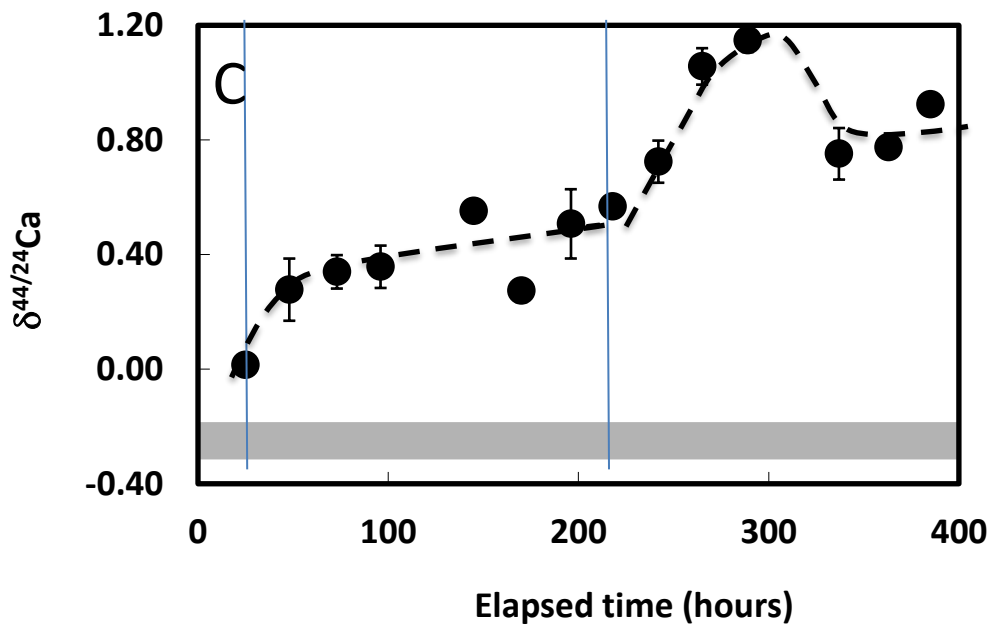
894



895



896

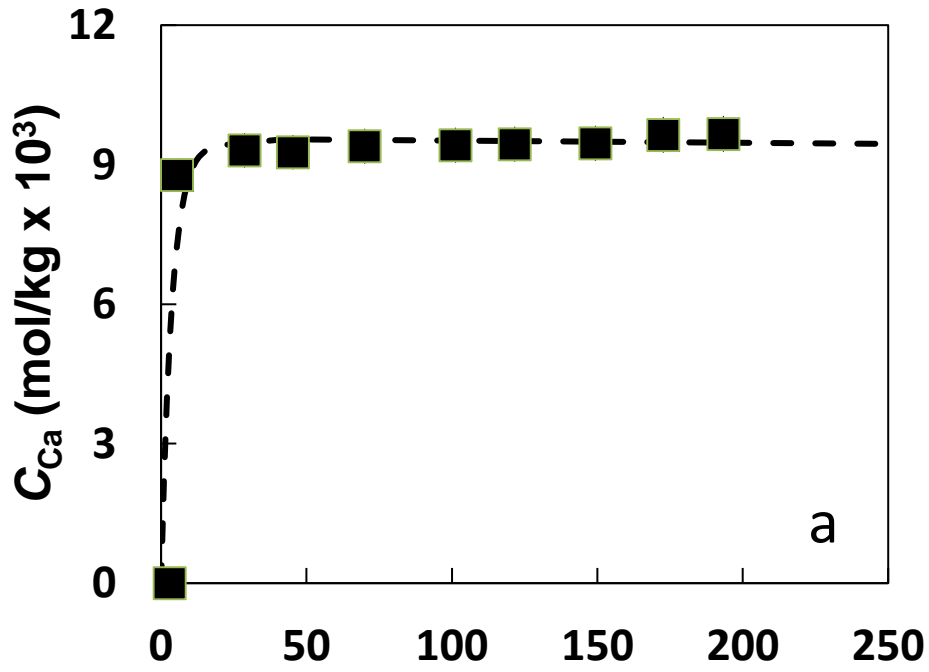


897

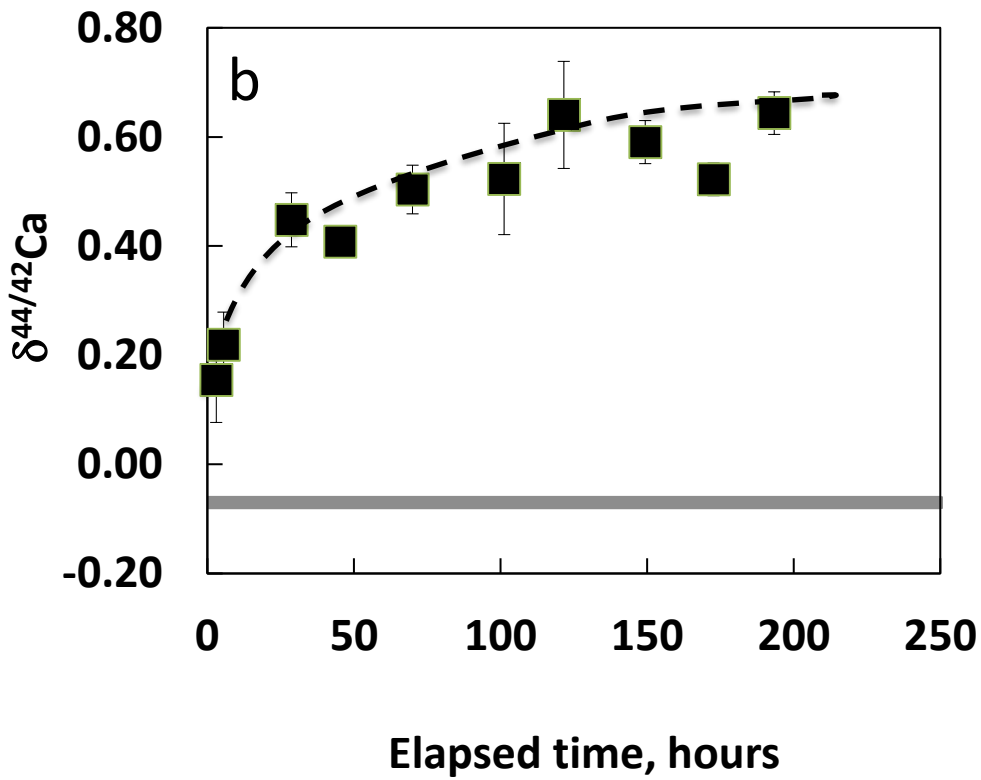
898

899

FIGURE 2:



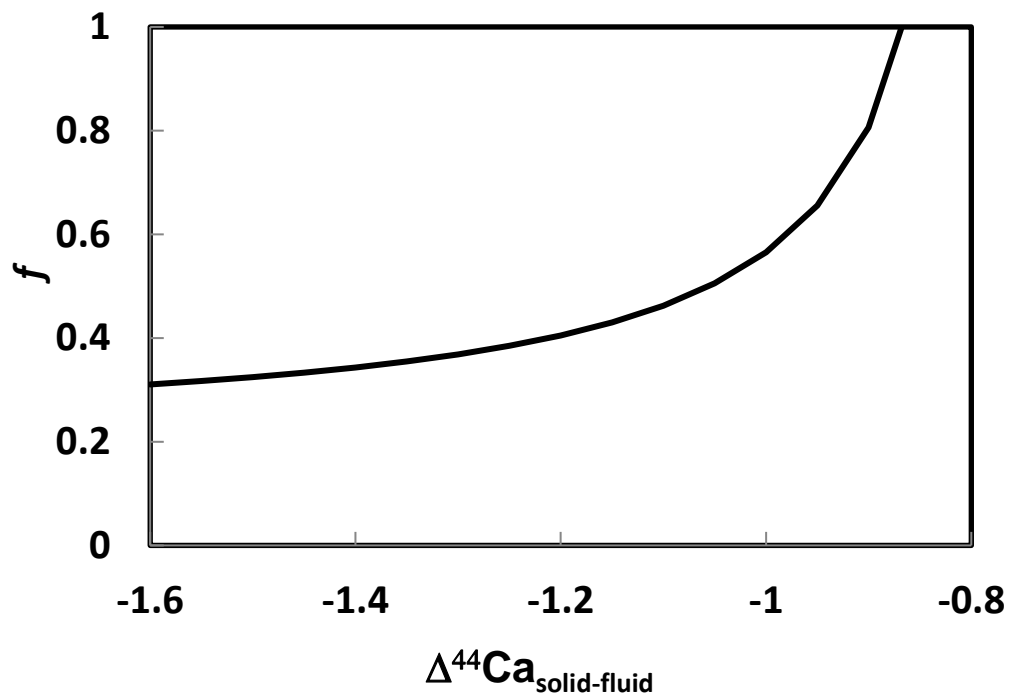
900



901

902

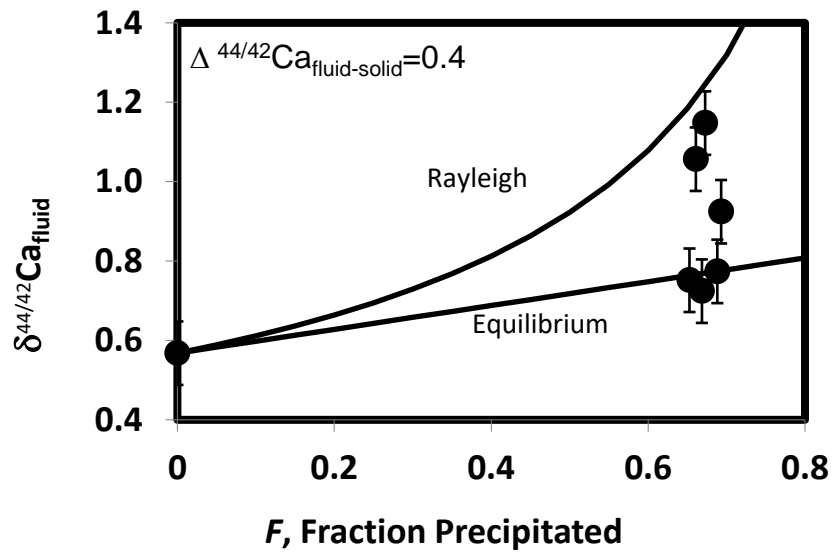
903 **Figure 3.**



904
905
906
907

Figure 4.

908



909

910 **Figure 5**

911